Int. J. Rock Mech. Min. Sci. & Geomech. Abstr. Vol. 28, No. 4, pp. 261–273, 1991
Printed in Great Britain.

0148-9062/91 $3.00 + 0.00

Pore Pressure Influence on Tensile Fracture Propagation in Sedimentary Rock

M. S. BRUNO†
F. M. NAKAGAWA†

Theoretical analysis and experimental results are presented to describe the influence of pore pressure on tensile fracture initiation and propagation direction. Fracture is influenced by both pore pressure magnitude on a local scale around the crack tip and by the orientation and distribution of pore pressure gradients on a global scale. Simple fracture initiation tests conducted on cylindrical limestone and sandstone rock samples are first described which support an effective stress law for tensile fracture initiation in very porous rocks. In other experiments, controlled fractures are propagated both mechanically and hydraulically across sandstone slabs subjected to non-uniform pore pressure fields. The fractures are shown to propagate towards regions of higher local pore pressure. Finally, the influence of pressure gradient induced body forces is demonstrated by generating fractures connecting two pore pressure source points. The experimental results are supported by poroelasticity and fracture mechanics analysis of the process, and may be applied to influence hydraulic fracture orientation in the field.

INTRODUCTION

A number of experimental studies have demonstrated that shear failure of porous rock is controlled by the conventional effective stress, equal to the total macroscopic stress σ_{ij} plus pore pressure p [1]. (*Tensile stresses and strains defined as positive.*) It is less clear, however, what role pore pressure plays in tensile rock fracture. The general assumption is that the conventional effective stress also controls tensile failure. For example, modified hydraulic fracture breakdown equations for porous materials typically assume failure occurs when the effective circumferential stress at the wellbore exceeds the material tensile strength T [2]:

$$\hat{\sigma}_{\theta\theta} = \sigma_{\theta\theta} + p > T. \tag{1}$$

Field evidence for pore pressure effects on fracture initiation and extension is sometimes ambiguous. Extending the effective stress concept to reservoir fracture problems, for example, would suggest that the additional borehole pressure required to initiate or extend hydraulic fractures should decrease with increasing reservoir pore pressure. Some field data indirectly support this conclusion. Fracture reopening and extension pressures tend to decrease with lower fluid injection rates, possibly due to greater fluid penetration into the formation [3]. This would be consistent with laboratory tests which show a decrease in breakdown pressure with greater fluid penetration [4, 5].

Other field evidence appears to contradict the effective stress law. Fracture propagation pressures tend to increase with higher reservoir pressure and decrease as the reservoir is drawn down [6, 7]. The problem is that pore pressure effects must be considered on both a local and global scale. While a local increase in pore pressure around the crack tip may enhance fracture extension, a global increase in pore pressure may inhibit fracture by increasing the compressive *in situ* stresses for the field [8, 9]. The general direction of fluid flow due to pore pressure differences must also be considered. Basic equilibrium principles may be applied to reveal that pore pressure gradients produce displacements in the same manner as body forces [10, 11].

A few researchers have investigated the influence of a uniform or symmetric pore pressure distribution on straight fracture propagation [12–14]. More complex questions concern the direction of fracture propagation within non-uniform pore pressure fields. Propagating rock fractures generally tend to orient themselves parallel to the maximum compressive far field stress, minimizing the energy required for extension [2, 4]. When the far field stress state is more uniform, *in situ* stress effects may not dominate fracture orientation. In such situations,

†Chevron Oil Field Research Co., P.O. Box 446, La Habra, CA 90633, U.S.A.

differences in pore pressure around the crack tip can influence fracture direction on a local scale while pressure gradient induced body forces can affect fracture orientation on a more global scale. Little theoretical or empirical evidence has been presented to deal with these problems.

The purpose of the present work is to investigate the influence of non-uniform pore pressure fields on fracture propagation direction. A brief review of poroelasticity theory is first presented and fracture mechanics principles are applied to describe the expected influence of pore pressure on fracture initiation and propagation direction. The validity of effective stress laws for tensile fracture in porous limestone and sandstone rocks is investigated using an apparatus similar to that employed in Bridgman's original "pinch-off" experiments [15]. Next, controlled fractures are propagated across porous rock slabs subjected to non-uniform pore pressure fields. In additional tests, a more uniform local pressure field is developed and fracture direction is controlled with global pressure distribution. The analysis and experimental data presented provide insight into the role pore pressure may play influencing hydraulic fracture extension and orientation in the field.

POROELASTICITY FIELD EQUATIONS

The influence of pore pressure on brittle failure has been discussed by several researchers, expanding on Terzaghi's early experiments with soils and saturated concrete [16,17]. It is often convenient to consider as separate state variables the pore fluid pressure p and total macroscopic stress σ_{ij}. The stress components are considered as average values acting over a scale which is large compared to the pore sizes, so that homogeneity is approximated. This continuum mechanics approach was first presented by Biot in 1941 [18]. The equations of poroelasticity have since been reformulated by Geertsma [19] and Cleary [20] in terms of material properties most easily measured in the laboratory, but for the present purposes no particular advantage is gained over the classical formulation which follows.

The elastic strain field is assumed to be linearly related to stress and the internal pore pressure, through the relation:

$$\epsilon_{ij} = \frac{1}{2\mu}(\sigma_{ij} - \tfrac{1}{3}\sigma_{kk}\delta_{ij}) + \frac{1}{9K}(\sigma_{kk}\delta_{ij}) + \frac{1}{3H}(p\delta_{ij}). \quad (2)$$

In this and following equations general tensor notation is employed with repeated indices indicating summation and comma notation used for partial derivatives. The first two terms in equation (2) describe the conventional strain dependence on the shear and bulk moduli of the porous rock, μ and K. The last term represents the strain due to variation in pore pressure p. This depends on a third material constant introduced by Biot [18], $1/H$, defining the material volume expansion due to changes in fluid pressure. The Kronecker delta term, δ_{ij}, is equal to 1 when $i = j$ and otherwise equal to zero, so that shear stresses and strains are unaffected by pore pressure. For small, linear deformation, the symmetric strain tensor components are defined with respect to the solid material displacement field u_i as follows:

$$\epsilon_{ij} = \tfrac{1}{2}(u_{i,j} + u_{j,i}). \quad (3)$$

The constitutive equations can be reduced to conventional elasticity form by defining an effective stress acting on the rock matrix:

$$\hat{\sigma}_{ij} = \sigma_{ij} + \alpha p \delta_{ij}, \quad (4)$$

where $\alpha = K/H$. For situations in which all void space is continuous and permeable to fluid filtration, the factor α can also be expressed in terms of the ratio of overall bulk modulus to modulus of the grains only, $\alpha = 1 - K/K_g$ [21]. Substitution of equation (4) into (2) will recover:

$$\epsilon_{ij} = \frac{1}{2\mu}(\hat{\sigma}_{ij} - \tfrac{1}{3}\hat{\sigma}_{kk}\delta_{ij}) + \frac{1}{9K}(\hat{\sigma}_{kk}\delta_{ij}), \quad (5)$$

which reduces to the conventional strain field for non-porous media when p is set to zero.

Deformation of the sold matrix effects the fluid flow through the rock pores, so that the solid mechanics and fluid mechanics equations become coupled. Let Φ represent the change in volume fraction of fluid contained in the pores. This quantity is related to the pressure and strain field through the following expression:

$$\Phi = \frac{p}{Q} + \alpha\epsilon_{kk}, \quad (6)$$

where the additional material parameter $1/Q$ defines the change in pore fluid volume with pressure under constant strain conditions [18]. Note that for a rock fully saturated with an incompressible fluid, $1/Q = 0$.

Conservation of momentum and mass principles may now be applied to determine the poroelasticity field equations in terms of stress equilibrium and fluid flow. For quasi-static situations in the absence of body forces, the stress equilibrium equations may be expressed as:

$$\sigma_{ij,j} = \hat{\sigma}_{ij,j} - \alpha p_{,i} = 0. \quad (7)$$

In terms of the equilibrium of effective stresses acting on the rock matrix the pressure gradient terms $-\alpha p_{,i}$ are equivalent to body forces. A difference in pore pressure acting on two sides of a volume element of rock must be counteracted by a change in effective stress within the rock material in order to maintain force equilibrium. The resulting influence on the rock deformation is analogous to the influence of temperature gradients in thermoelasticity problems [22].

To complete the analysis we require a set of field equations defining the flow of fluid through the rock pores. According to Darcy's law, the rate of fluid flow is proportional to the gradient of pore pressure at a point. By applying the continuity equation, which relates the rate of fluid flow into a small volume to the rate of increase of fluid volume, the following diffusion equation may be derived [18]:

$$kp_{,ii} = \frac{\partial\Phi}{\partial t} = \frac{1}{Q}\frac{\partial p}{\partial t} + \alpha\frac{\partial\epsilon_{kk}}{\partial t}, \quad (8)$$

where k represents the permeability of the rock matrix.

In summary, equations (7) and (8) provide a complete set of governing equilibrium and diffusion equations for a poroelastic medium, with strains related to stresses, displacements and pore pressure through equations (2–6). In general the fluid pressure and stress–strain fields are coupled, so that analytic solutions are available for just a few simplified situations (see for example [11]). For most practical problems numerical solution techniques must be employed. In the following sections we will assume that the general nature of a pore pressure field is known at a given point in time and we will investigate its influence on fracture initiation and propagation direction.

FRACTURE INITIATION AND EXTENSION THEORY

Fluid saturated rock failure may be investigated from two different perspectives. In the traditional strength of materials approach, elasticity equations are applied to determine a general state of stress, and failure is assumed to occur when the conventional effective stress ($\alpha = 1$) exceeds the tensile strength of the material. A few previous studies on low permeability rocks have supported this assumption, including Jaeger's "pinch-off" experiments on dolerite, marble and quartzite [23], and recent preliminary hollow cylinder tests on granite conducted by Schmitt and Zoback [24].

A second approach to rock fracture is based on thermodynamic principles described by Griffith [25]. Starting with the first law of thermodynamics (conservation of energy), Griffith postulated that for an increment of crack extension the change in potential energy of deformation must equal the amount of energy required to create the new crack surface. A suggested by Irwin [26] and Orowan [27], the required energy includes not only surface energy density γ but also any additional thermal or plastic deformation energy d dissipated during crack extension. Assuming that the crack is extended under conditions of either prescribed force or prescribed displacement, the failure law may be summarized as:

$$\left[\frac{\mathrm{d}U}{\mathrm{d}A}\right] = \gamma + d = G_c, \tag{9}$$

where G_c is the *critical strain energy release rate*, $\mathrm{d}U$ is the change in internal strain energy and $\mathrm{d}A$ represents the change in total crack surface area. The strain energy release rate is directly related to other parameters commonly used in fracture mechanics, including the crack tip stress intensity factor, described by Irwin [28], and the path independent J-integral described by Rice [29].

Several researchers have applied fracture mechanics principles to hydraulic fracture problems (e.g. [30–32]). Previous works have included the effects of internal crack fluid pressure on the crack tip stress intensity factor, and the role of external pore pressure on driving fluid leakoff from the crack [31,32]. The following analysis considers an additional effect—the contribution of pore pressure to the change in total potential energy necessary for fracture extension. Though not formalized, the pore pressure contribution to fracture extension has been mentioned by Cleary [13], who applied stress relaxation and crack closure arguments.

Consider a poroelastic planar body of unit thickness, with area A bounded by a surface S. The strain energy per unit thickness for the system may be expressed:

$$U = \tfrac{1}{2}\int_A (\sigma_{ij}\epsilon_{ij} + p\Phi)\mathrm{d}A. \tag{10}$$

Substituting equations (3) and (6) into (10) will yield:

$$U = \tfrac{1}{2}\int_A \left(\sigma_{ij}u_{i,j} + \alpha p u_{i,i} + \frac{p^2}{Q}\right)\mathrm{d}A. \tag{11}$$

Making use of the equilibrium equations (7), we may rewrite this expression as:

$$U = \tfrac{1}{2}\int_A \left[(\sigma_{ij}u_i)_{,j} + (\alpha p u_i)_{,i} - \alpha p_{,i}u_i + \frac{p^2}{Q}\right]\mathrm{d}A. \tag{12}$$

The divergence theorem may now be applied to equate the first two terms within the volume integral to traction vectors applied over the surface:

$$U = \tfrac{1}{2}\left[\int_S (\sigma_{ij}n_j + \alpha p n_i)u_i \mathrm{d}S + \int_A \left(\frac{p^2}{Q} - \alpha p_{,i}u_i\right)\mathrm{d}A\right], \tag{13}$$

where n_i are the direction cosines of the unit normal to the surface S.

Let us evaluate the difference in potential energy for two equilibrium states, shown schematically in Fig. 1. We will follow the general line of reasoning applied by Rice [28] and Kannenen and Popelar [33] for elastic fracture, with modifications required to account for the pore pressure field. In state 1 the poroelastic body contains a crack of length a and in state 2 the body contains a crack of length $a + \Delta a$, which adds an amount ΔS to the original boundary. This additional surface in state 2 is assumed to be traction free. Cartesian and polar coordinate systems are defined with origins at the crack tip as shown. Let us denote the stress and displacement field for state 1 by σ_{ij} and u_i, and for state 2 by σ'_{ij} and u'_i. Along the boundary S we will either prescribe the traction vectors $T_i = \sigma_{ij}n_j = \sigma'_{ij}n_j$ or con-

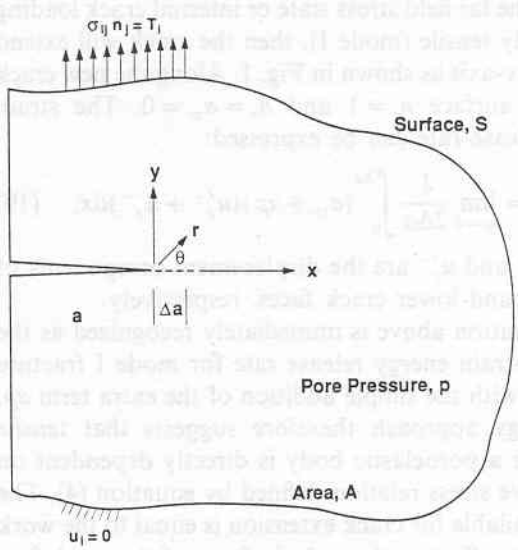

Fig. 1. Planar tensile fracture extension.

strain the displacement vectors $u_i = u_i' = 0$, and we will either prescribe the pressure or the fluid flux. The boundary conditions and the pore pressure field are assumed to remain fixed during crack extension from state 1 to state 2. The change in strain energy due to crack extension may be expressed:

$$\Delta U = \tfrac{1}{2}\left[\int_S (T_i + \alpha p n_i)(u_i' - u_i)\mathrm{d}S - \int_A \alpha p_{,i}(u_i' - u_i)\mathrm{d}A\right]. \quad (14)$$

Next note that the displacement field u_i of the first state is kinematically admissible for the second state. The displacement field u_i' of the second state is also kinematically admissible for the first state, if we include the stress and pore pressure components acting on the new crack surface ΔS. The principle of virtual work therefore requires:

$$\int_S (T_i + \alpha p n_i)u_i'\mathrm{d}S + \int_{\Delta S} (\sigma_{ij}n_j + \alpha p n_i)u_i'\mathrm{d}S + \int_A \left(\frac{p^2}{Q} - \alpha p_{,i}\right)u_i'\mathrm{d}A = \int_A (\sigma_{ij}\epsilon_{ij}' + p\Phi')\mathrm{d}A. \quad (15)$$

Betti's reciprocal theorem further requires that:

$$\int_A (\sigma_{ij}\epsilon_{ij}' + p\Phi')\mathrm{d}A = \int_A (\sigma_{ij}'\epsilon_{ij} + p\Phi)\mathrm{d}A = \int_S (T_i + \alpha p n_i)u_i\mathrm{d}S + \int_A \left(\frac{p^2}{Q} - \alpha p_{,i}\right)u_i\mathrm{d}A. \quad (16)$$

Equations (14), (15) and (16) may be combined to conclude that:

$$\Delta U = -\tfrac{1}{2}\int_{\Delta S} (\sigma_{ij}n_j + \alpha p n_i)u_i'\mathrm{d}S. \quad (17)$$

Finally, application of equation (9) allows us to express the Griffith strain energy release rate due to a virtual crack extension Δa with the following:

$$G = \lim_{\Delta a \to 0}\left|\frac{\Delta U}{\Delta a}\right| = \lim_{\Delta a \to 0}\frac{1}{2\Delta a}\int_{\Delta S} (\sigma_{ij}n_j + \alpha p n_i)u_i'\mathrm{d}S. \quad (18)$$

When the far field stress state or internal crack loading is primarily tensile (mode I), then the crack will extend along the x-axis as shown in Fig. 1. Along the new crack extension surface $n_y = 1$ and $n_x = \sigma_{xy} = 0$. The strain energy release rate can be expressed:

$$G = \lim_{\Delta a \to 0}\frac{1}{2\Delta a}\int_0^{\Delta a} (\sigma_{yy} + \alpha p)(u_y'^{+} + u_y'^{-})\mathrm{d}x, \quad (19)$$

where $u_y'^{+}$ and $u_y'^{-}$ are the displacement components of the upper and lower crack faces, respectively.

The equation above is immediately recognized as the standard strain energy release rate for mode I fracture extension with the simple addition of the extra term αp. This energy approach therefore suggests that tensile fracture in a poroelastic body is directly dependent on the effective stress relation defined by equation (4). The energy available for crack extension is equal to the work done by the effective stress $\hat{\sigma}_{yy}$ in front of the crack face acting over the new crack tip opening displacement.

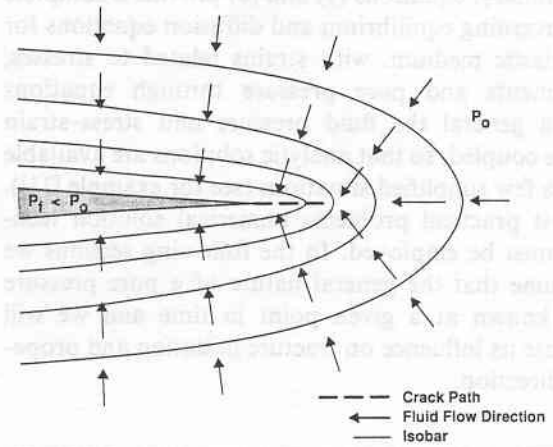

Fig. 2. Fluid flow directed towards fracture extension inhibits growth.

While the magnitude of pore pressure at the crack tip contributes directly to the strain energy release rate, the orientation of any pore pressure gradient field also influences fracture extension. As described in equation (7) of the second section, the pressure gradient terms $-\alpha p_{,i}$, enter the equilibrium equation for effective stresses on the rock matrix in the form of induced body forces. The pressure gradient field may either increase or decrease the effective stress, and hence the strain energy release rate, depending on its direction with respect to the fracture.

For example, consider a situation in which fluid flows inwards towards an extending fracture tip as shown schematically in Fig. 2. The induced forces are compressive and roughly perpendicular to the fracture axis, and their effect will be to reduce the effective stress and the strain energy available for crack extension. Additional work is required to displace the volume around the crack tip against the direction of pressure gradient induced body forces. Such an influence has been described as "pore fluid suction" of "back stress" to account for high-speed fracture stabilization [13, 32].

Next consider a situation where fluid flow is directed outwards along a potential fracture path, such as along the line connecting two pressure sources as shown in Fig. 3. The induced forces are tensile and roughly perpendicular to the potential fracture path, and their effect will be to increase the effective stress and the strain energy available for fracture creation. Such an effect is demonstrated experimentally in the penultimate section of this paper.

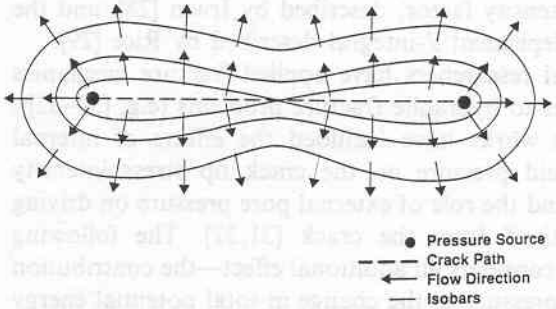

Fig. 3. Fluid flow directed away from potential fracture path enhances growth.

FRACTURE INITIATION EXPERIMENTS

To investigate the validity of the effective stress law for tensile fracture in a uniform pore pressure field, experiments were conducted on limestone and sandstone samples using an apparatus similar to that employed in Bridgeman's original "pinch-off" tests [15]. Jaeger and Cook applied a similar procedure to produce tensile fractures in dolerite, marble and quartzite [23]. Cylindrical samples 2.5 cm dia and 22 cm long are placed in the vessel as shown in Fig. 4. Radial seals are positioned near the ends and can seal either directly on the core surface or on an epoxy coating applied over a short region near the ends. Generous seal lubricant is applied to minimize axial load caused by sealing friction. Water is injected into the annular chamber between the core and vessel inside diameter at a known pressure P. The ends of the core are open to atmosphere so that fluid flows into the sample along the radial surface and out of each end. The boundary conditions for the sample may be expressed as:

$$\sigma_{rr} = -P \quad \text{at } r = R; \qquad \sigma_{zz} = 0 \quad \text{at } z = 0, L. \tag{20}$$

The axisymmetric loading conditions require that no shear stresses act throughout the body. Given enough time to equilibrate, the pore pressure within the sample will be uniformly equal to P, except for the regions within about a half diameter from the cylinder ends. The internal stresses over most of the core sample are therefore:

$$\sigma_{rr} = \sigma_{\theta\theta} = -P; \qquad \sigma_{zz} = 0, \tag{21}$$

$$\hat{\sigma}_{rr} = \hat{\sigma}_{\theta\theta} = (\alpha - 1)P; \quad \hat{\sigma}_{zz} = \alpha P. \tag{22}$$

Note that while the longitudinal total stress $\sigma_{zz} = 0$, the longitudinal effective stress in the sample is tensile and equal to αP. If the fluid pressure is slowly increased, so that quasi-steady state conditions are maintained, a fracture perpendicular to the z-axis should occur when the effective stress exceeds the material tensile strength. The theoretical analysis described earlier suggests that failure should occur at a fluid pressure $P = \frac{1}{\alpha}T$.

Fracture tests were performed on samples of Boise limestone and Berea sandstone. The porosity of the limestone samples was 14% and the porosity of the sandstone samples was about 22%. In all cases a single tensile fracture occurred perpendicular to the core axis and from about 1–3 core diameters away from the seals. Failure was often indicated by an audible "popping" sound from the core and an immediate loss of system pressure. The pressure at fracture recorded for five limestone samples averaged 3100 kPa with a maximum deviation of 207 kPa. The pressure at fracture recorded for four sandstone samples averaged 1100 kPa, with a maximum deviation of 138 kPa.

Published tensile strengths for limestone and sandstone samples vary by up to two orders of magnitude. In order to establish comparative strength values for these specific materials, direct pull tension tests were performed using the arrangement illustrated in Fig. 5. The samples were bonded to end fixtures with epoxy. Axial load is transferred to the sample through the chain and pin arrangement shown, in an attempt to minimize bending stresses in the sample. The central region of the samples was slightly tapered to produce tensile failure away from the ends. The average tensile strength for five limestone samples measured with this technique was 2930 kPa, with a maximum deviation of about 455 kPa. The average tensile strength for five sandstone samples was 931 kPa, with a maximum deviation of about 166 kPa. Note that the deviation in failure strength measured with this technique is larger than that measured with the pore fluid method. These results are summarized in Tables 1 and 2.

The data show that the pore pressure required for failure is close to and perhaps slightly higher than the material tensile strength. Some form of effective stress clearly controls failure. Rice and Cleary report a poroelastic coefficient for Berea sandstone, $\alpha = 0.79$ [10], while Haimson and Fairhurst report a value $\alpha = 0.85$ [34]. These values are consistent with the data presented above, assuming that tensile fracture is controlled by the general effective stress defined in equation (4). The large variability in measured data, however, does not allow us to completely rule out the possibility that tensile failure is more simply dependent on the conventional effective stress, $\hat{\sigma}_{zz} = \sigma_{zz} + p \geqslant T$. The important point is that these experiments confirm the direct influence of pore pressure magnitude on tensile fracture initiation in high-porosity rocks.

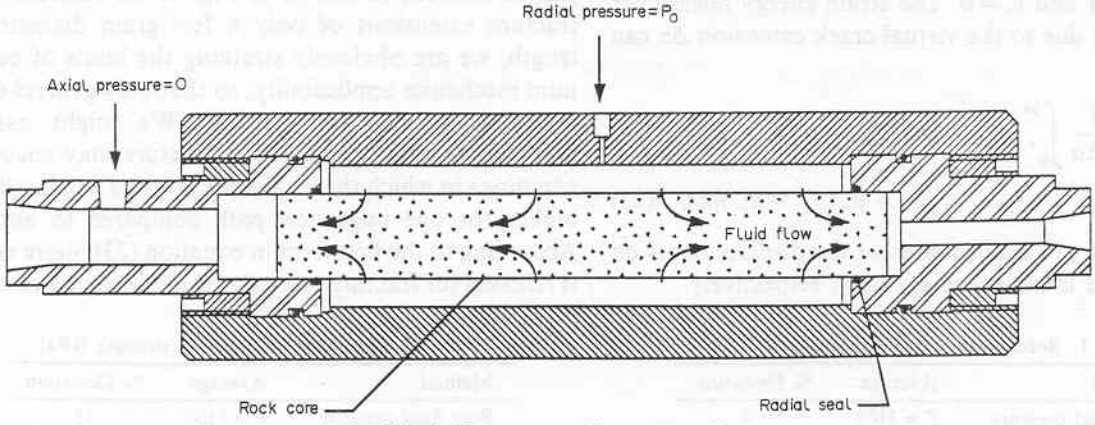

Fig. 4. Pore pressure fracture vessel.

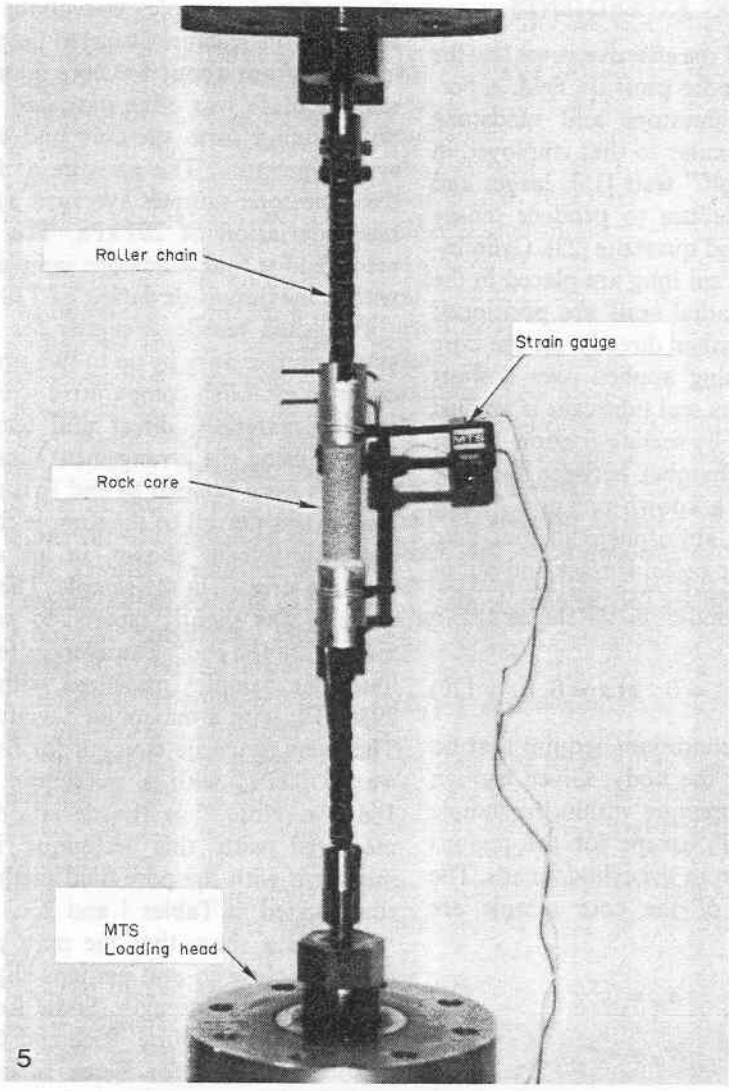

Fig. 5. Direct pull tensile test apparatus.

FRACTURE PROPAGATION IN NON-SYMMETRIC PRESSURE FIELDS

When the loading or the pore pressure distribution is not oriented perpendicular to the crack axis, then fracture propagation may extend at some angle to the original fracture axis. Let us examine the energy release rate for fracture extension along a radial path at some angle θ_e. Polar coordinates centred at the original crack tip are defined as in Fig. 1. Along the crack extension surface, $n_\theta = 1$ and $n_r = 0$. The strain energy release per unit thickness due to the virtual crack extension $\Delta\alpha$ can be expressed:

$$G = \lim_{\Delta a \to 0} \frac{1}{2\Delta a} \int_0^{\Delta a} [(\sigma_{\theta\theta} + \alpha p)(u_\theta'^{+} - u_\theta'^{-}) + \sigma_{r\theta}(u_r^{+} - u_r^{-})]\mathrm{d}r, \quad (23)$$

where $u_i'^{+}$ and $u_i'^{-}$ again represent the displacements on the upper and lower crack surfaces, respectively.

Fracture extension will occur when $G \geqslant G_c$ in the direction θ_e for which G is maximum. This may be influenced by small differences in pressure distribution around the crack tip. For example, consider a situation in which a fluid pressure gradient is directed perpendicular to the axis of a propagating fracture, which is otherwise loaded in a primarily tensile manner. In sedimentary rock, fracture propagation on the microstructure level primarily traverses grain boundaries in a jagged fashion, as shown in Fig. 6. To consider small fracture extensions of only a few grain diameters in length, we are obviously straining the limits of continuum mechanics applicability, so that only general qualitative arguments are justified. We might assume, however, that the propagating fracture may encounter situations in which the local pore pressure will be slightly higher for one migration path compared to another. According to the first term in equation (23), more energy is released for fracture extension into the region of higher

Table 1. Boise limestone tensile strength (kPa)

Method	Average	% Deviation
Pore fluid pressure	$T = 3100$	7
Direct pull test	$T = 2930$	16

Table 2. Berea sandstone tensile strength (kPa)

Method	Average	% Deviation
Pore fluid pressure	$P = 1100$	13
Direct pull test	$T = 931$	18

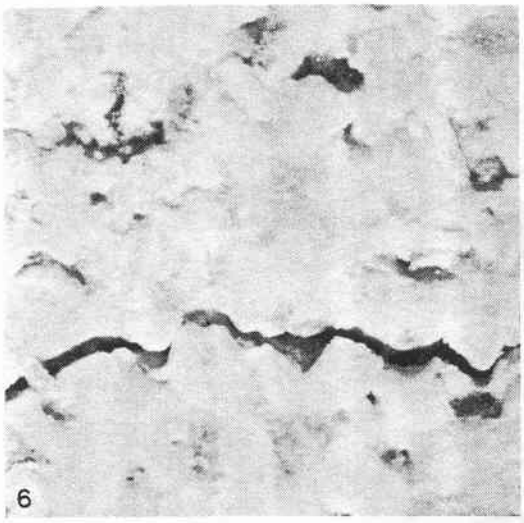

Fig. 6. Tensile fractures traverse grain boundaries.

pore pressure. Assuming that the first term in equation (23) dominates the strain energy release rate, the propagating fracture should gradually turn towards the direction of higher pore pressure.

The validity of this last assumption is reasonable, but difficult to confirm. A few numerical solutions based on Muskhelishvili's potential formulation have been presented for the stress and strain fields around branched crack subject to far field mode I loading, as discussed by Lo [35]. For branch angles less than about 45°, the calculated mode I stress intensity factor at the branch tip is much larger than the mode II factor [35]. This implies that the normal stresses and displacements will be much larger than the shear stresses and displacements along the crack surface. A pressure gradient directed roughly perpendicular to the main fracture axis will have an almost neutral effect. That is, induced body forces will act against the displacement field on one side of the extension and with the displacement field on the other. The result is that these types of local pressure gradient forces have only a small influence on fracture extension direction. It is primarily the difference in pore pressure magnitude around the crack tip that will tend to turn a fracture towards regions of higher pore pressure. These general arguments are consistent with experimental results described in the next section.

FRACTURE PROPAGATION EXPERIMENTS

We have devised several laboratory experiments to demonstrate the influence of pore pressure on fracture propagation direction. Square slabs of Colton sandstone, 15.2 cm on a side and of thickness varying from 0.95 to 2.54 cm, are placed between rubber gaskets and metal plates in a sandwich type assembly shown in Figs 7a and b. The porosity of the sandstone samples is about 11% and the permeability is about 0.04 mDa. Fluid is injected into the rock slab at varying locations and produced from other locations to establish non-uniform pore pressure fields. The fluid used is mineral oil, which is chemically inert to the rock material. Low-permeability samples were chosen so that controlled diffusion patterns could be established. Fractures can be propagated across the non-uniform pressure field in two manners, either by mechanical separation of a notch at the top of the sample or by hydraulic fracture from one of the injection ports.

In the first set of experiments a pressure gradient is established across the lower portion of the rock slab by injecting fluid into one port and producing fluid from the second. The fluid is contained within the rock pores by applying uniform torque on the bolts around the rock periphery to compress the plate assembly, resulting in radial fluid diffusion which is uniform across the slab thickness. The computer control and data acquisition system used, shown schematically in Fig. 8, is capable of measuring and controlling fluid flow rates with an accuracy of 0.001 cm^3/min and pressure with an accuracy of about 10 kPa.

A fracture is propagated downward by driving a wedge into a vertical slot at the top of the sample, as illustrated schematically in Fig. 8. The wedge provides not only mode I tensile loading onto the crack tip, but also a downward compressive load onto the rock slab. The bottom of the slab rests on the surface of the lower assembly bolt. The resulting compressive point loading in the vertical direction essentially creates the rectangular equivalent of a Brazilian disk test. Lateral tensile stresses proportional to the compressive point load are generated over the central portion of the sample, as described by Goodier [36]. In the absence of pore pressure effects the fracture should propagate in a roughly straight path, as shown in Fig. 9a.

A non-uniform pressure field may be established across the lower potion of the sample to demonstrate the influence of pore pressure. We recognize that dynamic effects on crack branching are not easily controlled or measurable in these tests, so that only qualitative trends in fracture orientation will be discussed. Fluid is injected into one of the lower ports at a constant pressure, while the other port is maintained at atmospheric conditions. When fluid begins to drain from the production port, then a varying pressure field is known to be established across the sample. At this point the vertical loading on the mechanical wedge is increased at a constant rate so as to produce fracture in about 3–5 min. As shown in Fig. 9b, the propagating fracture is seen to turn towards the region of high pore pressure before eventually turning back towards the bottom point contact. This behaviour supports the theoretical analysis presented earlier. Several experiments were conducted with a maximum pore pressure at the inlet port ranging from 500 to 1400 kPa. Although the amount of fracture path deviation was not always consistent for the same pressure gradient, higher injection (pore) pressures consistently produced the greatest amount of fracture turning.

The slab thickness was varied from 0.95 to 2.54 cm to investigate the influence of surface effects. These were found to be insignificant. The diameters of the injection port hole in the rock slabs were varied from 6.3 to

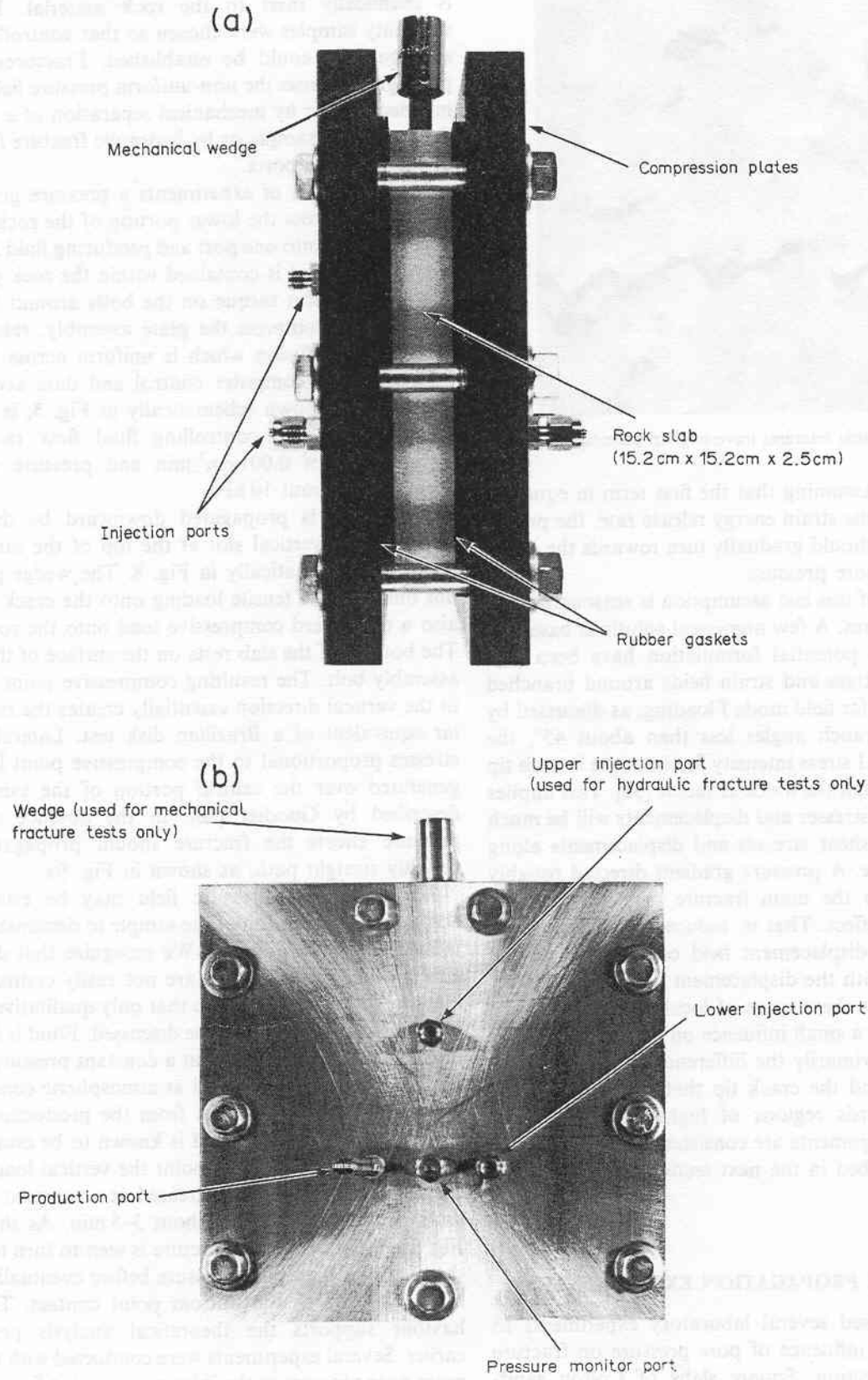

Fig. 7. Slab fracture apparatus: (a) side view; and (b) front view.

4.7 mm to reduce stress fields caused by pressure loading on the hole surfaces. This also produced no changes. The tangential tensile stress induced around a pressurized hole falls off with the square of the radius, so that at the midpoint of the sample specimen this stress contribution is less than 2% of the maximum fluid pressure. One test was conducted with no holes through the sample (fluid was injected into circular surfaces on opposite faces of the slab). In this test the fracture also turned towards the higher pore pressure zone.

In an effort to examine fracture propagation under simpler boundary conditions and better controlled stress

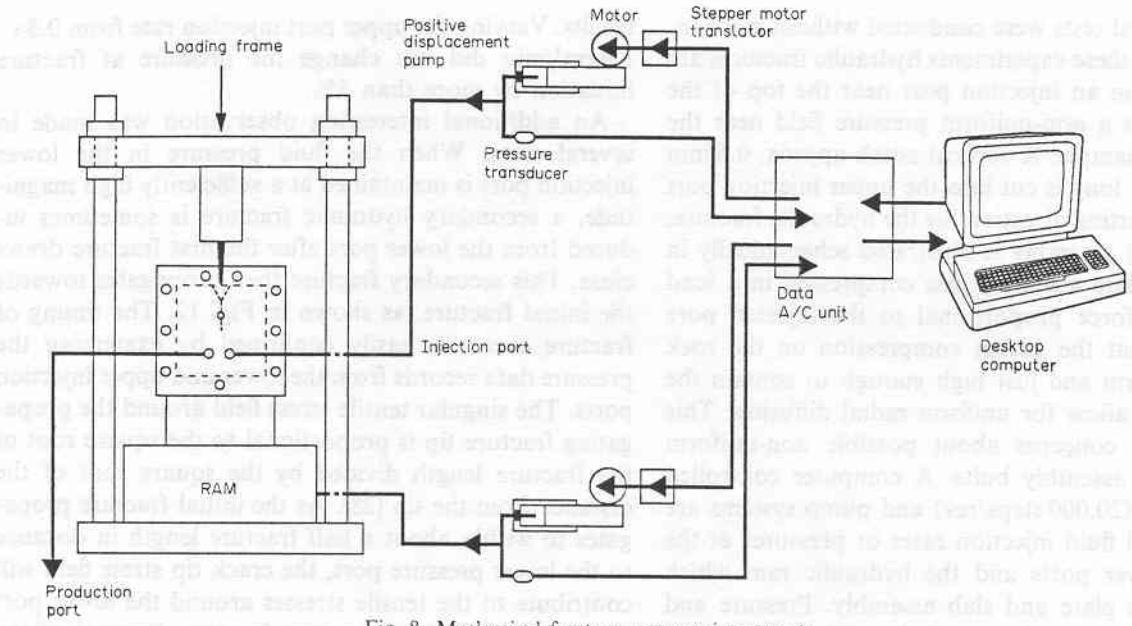

Fig. 8. Mechanical fracture propagation system.

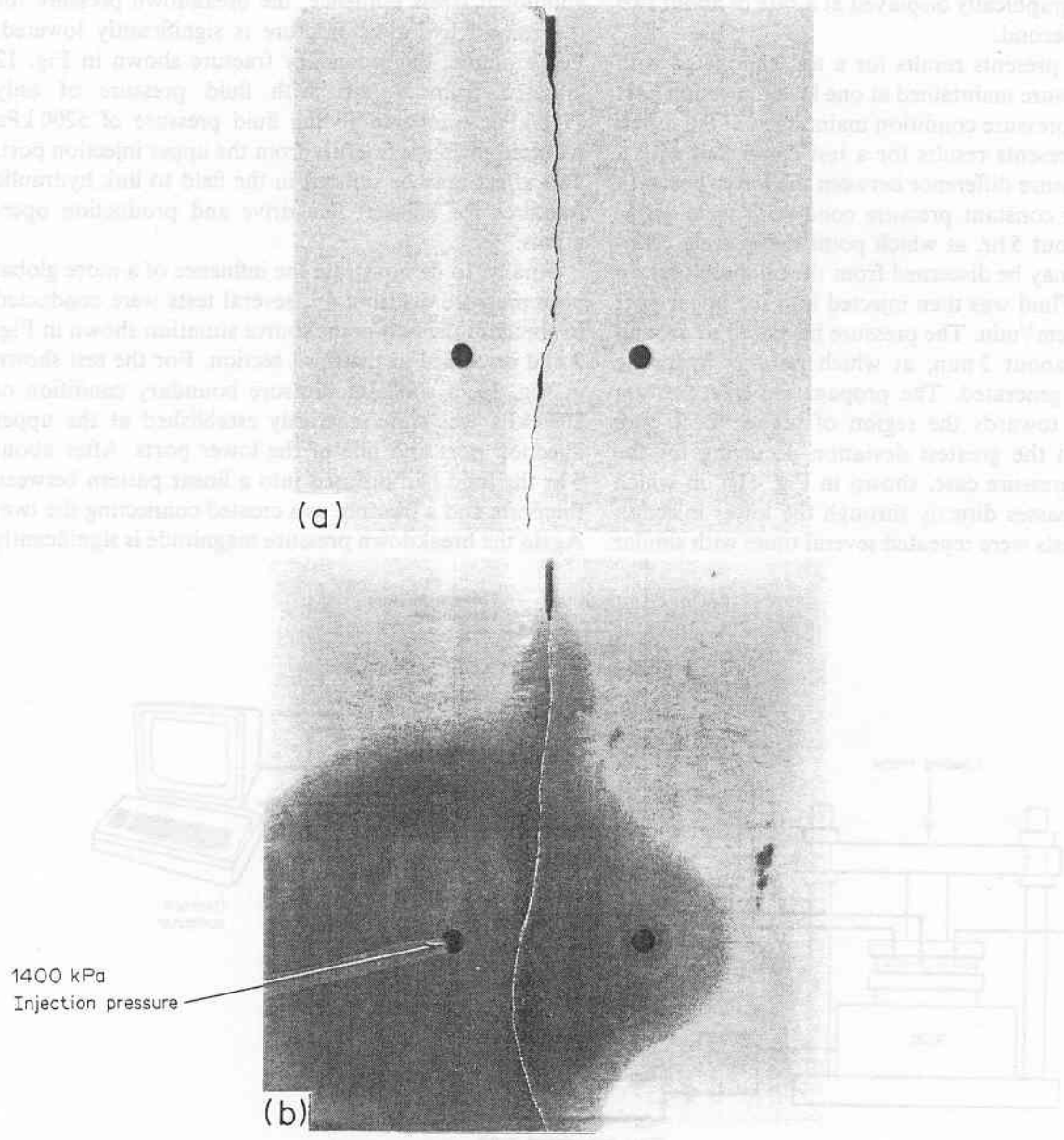

Fig. 9. (a) Fracture in absence of pore pressure effects; and (b) fracture turns towards region of high pore pressure.

states, additional tests were conducted without mechanical loading. In these experiments hydraulic fractures are propagated from an injection port near the top of the sample towards a non-uniform pressure field near the bottom of the sample. A vertical notch approx. 0.6 mm wide and 6 mm long is cut into the upper injection port to provide a starting direction for the hydraulic fracture. The system test assembly is illustrated schematically in Fig. 10. The plate assembly was compressed in a load frame with a force proportional to the injected pore pressure, so that the gasket compression on the rock slab was uniform and just high enough to contain the pore fluid and allow for uniform radial diffusion. This eliminates any concerns about possible non-uniform torque on the assembly bolts. A computer controlled stepper motor (20,000 steps/rev) and pump systems are used to control fluid injection rates or pressures at the upper and lower ports and the hydraulic ram which compresses the plate and slab assembly. Pressure and flow rate information is recorded, used for feedback control, and graphically displayed at a rate of about two samples per second.

Figure 11a presents results for a test conducted with 1400 kPa pressure maintained at one lower injection port and ambient pressure condition maintained at the other. Figure 11b presents results for a test conducted with a 1730 kPa pressure difference between the lower ports. In each case the constant pressure conditions were maintained for about 5 hr, at which point the existing diffusion pattern may be discerned from the oil discoloration of the rock. Fluid was then injected into the upper port at a rate of 2 cm^3/min. The pressure increased to around 5200 kPa in about 3 min, at which point a hydraulic fracture was generated. The propagating fractures are seen to turn towards the region of higher local pore pressure, with the greatest deviation occurring for the higher pore pressure case, shown in Fig. 11b, in which the fracture passes directly through the lower injection port. These tests were repeated several times with similar results. Varying the upper port injection rate from 0.5 to 3.0 cm^3/min did not change the pressure at fracture initiation by more than 5%.

An additional interesting observation was made in several tests. When the fluid pressure in the lower injection port is maintained at a sufficiently high magnitude, a secondary hydraulic fracture is sometimes induced from the lower port after the first fracture draws close. This secondary fracture then propagates towards the initial fracture, as shown in Fig. 12. The timing of fracture events is easily confirmed by examining the pressure data records from the lower and upper injection ports. The singular tensile stress field around the propagating fracture tip is proportional to the square root of the fracture length divided by the square root of the distance from the tip [28]. As the initial fracture propagates to within about a half fracture length in distance to the lower pressure port, the crack tip stress field will contribute to the tensile stresses around the lower port and can induce the secondary fracture. Because of the additional stress influence, the breakdown pressure for the second hydraulic fracture is significantly lowered. For example, the secondary fracture shown in Fig. 12 initiated from a port with fluid pressure of only 1730 kPa, compared to the fluid pressure of 5200 kPa required to create fracture from the upper injection port. This effect may be utilized in the field to link hydraulic fractures for efficient line drive and production operations.

Finally, to demonstrate the influence of a more global pore pressure distribution, several tests were conducted to simulate the two-point source situation shown in Fig. 3 and discussed in the third section. For the test shown in Fig. 13, a constant pressure boundary condition of 2070 kPa was simultaneously established at the upper injection port and one of the lower ports. After about 5 hr the fluid had diffused into a linear pattern between the ports and a fracture was created connecting the two. Again the breakdown pressure magnitude is significantly

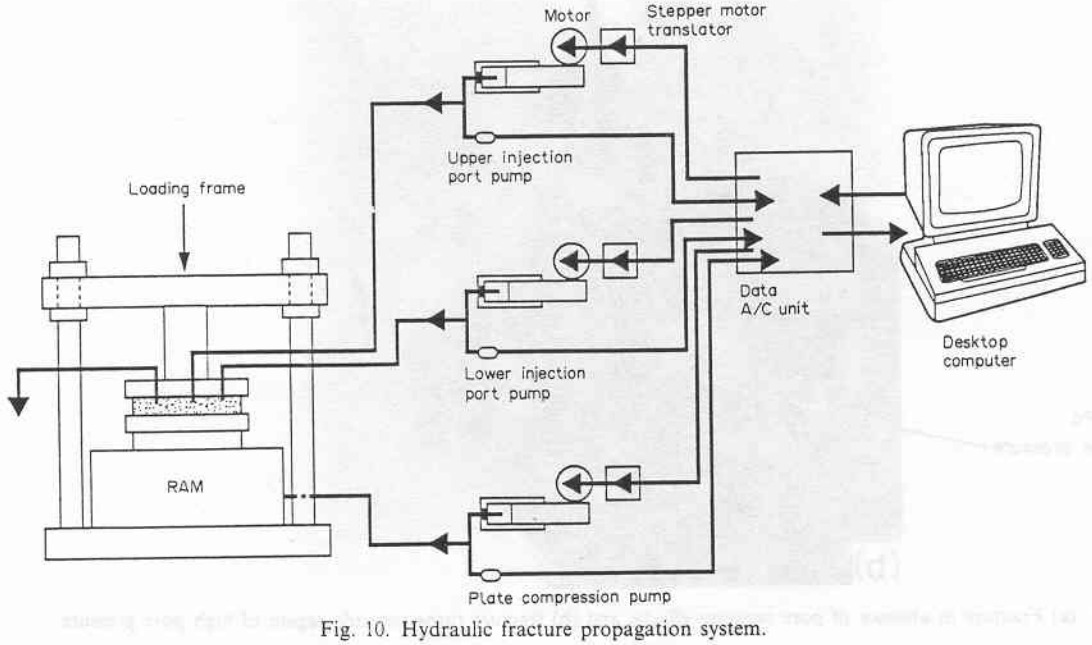

Fig. 10. Hydraulic fracture propagation system.

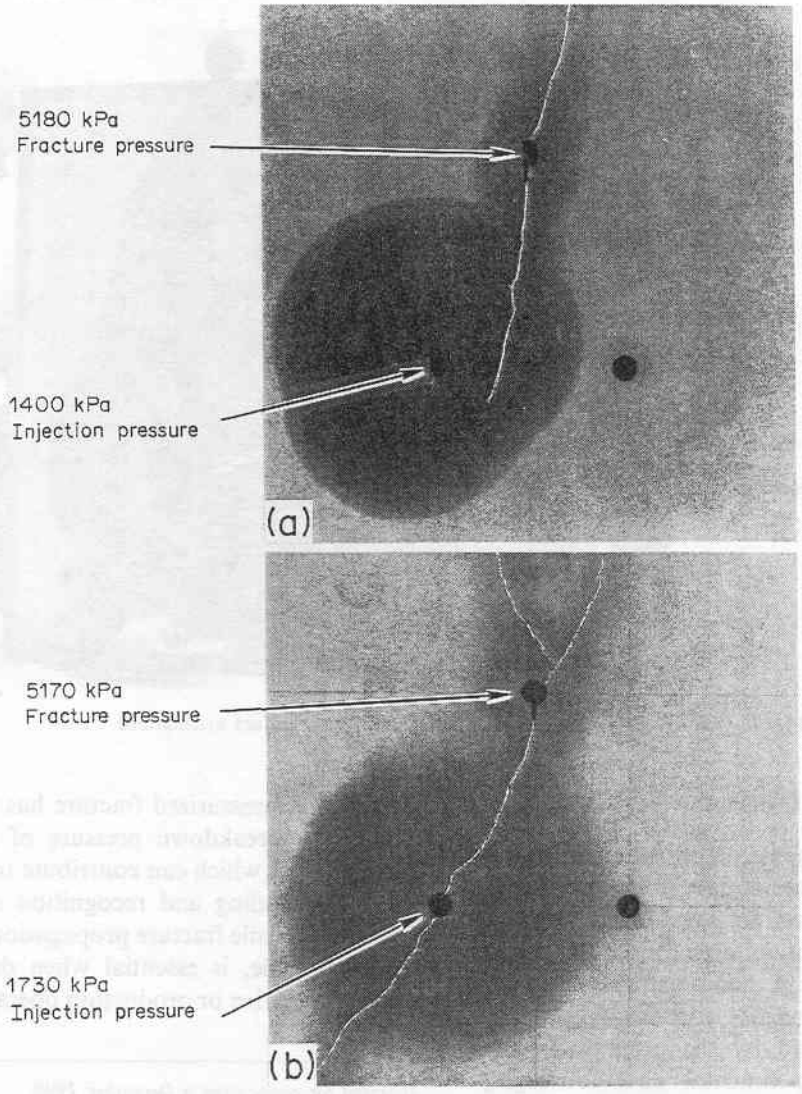

Fig. 11. (a) Fracture turning towards injection port (1400 kPa); and (b) fracture propagating through injection port (1730 kPa).

lower than the pressure required for fracture initiation from a single port or multiple ports in the absence of a preferentially aligned pore pressure field. The experiments clearly demonstrate that pressure gradient induced body forces can effect both fracture initiation and orientation.

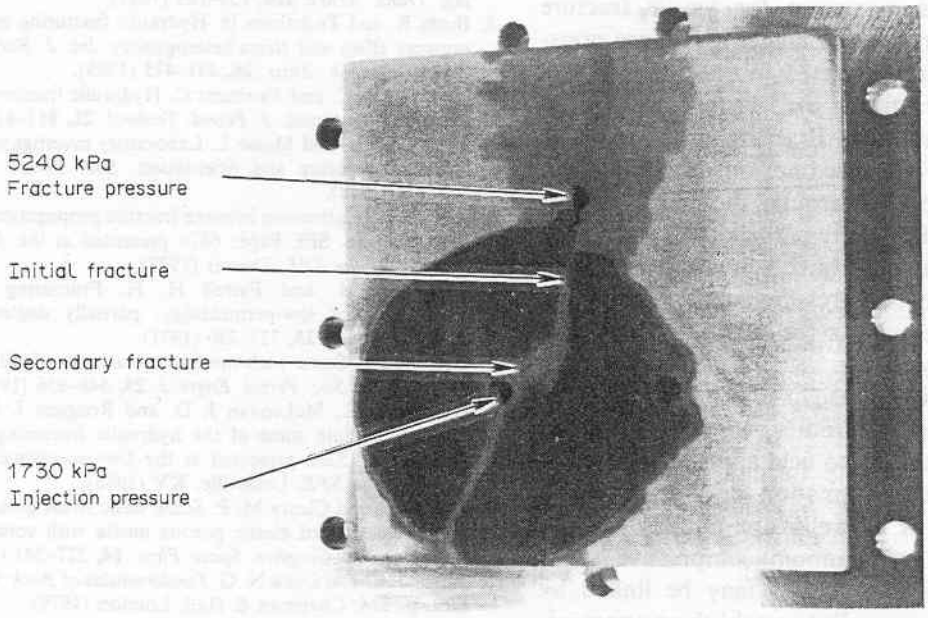

Fig. 12. Induced secondary fracture from injection port.

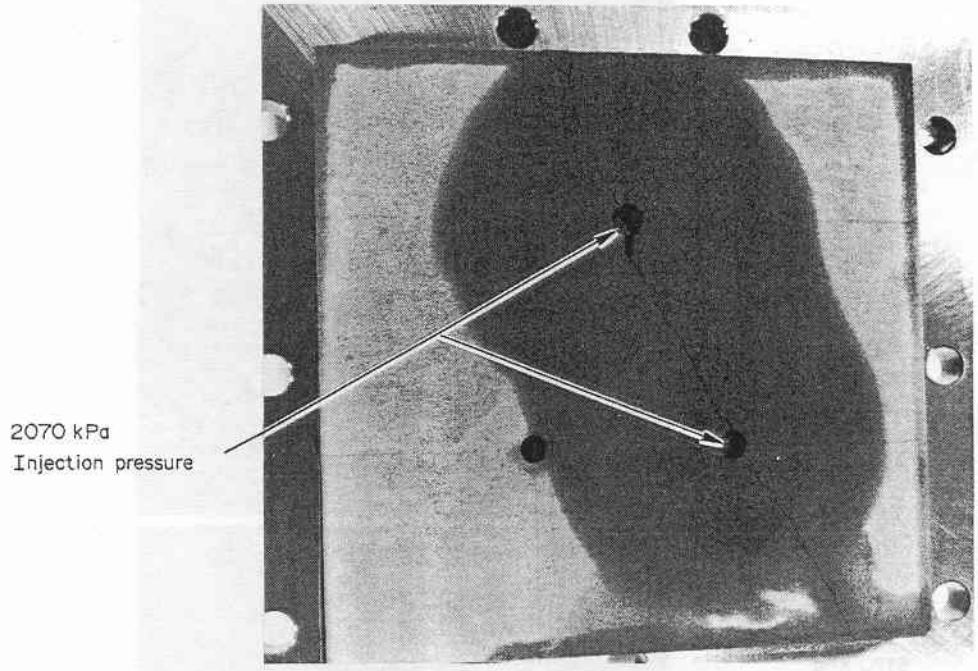

Fig. 13. Global pore pressure distribution influences fracture orientation.

CONCLUSIONS

The analysis and experiments described in this paper demonstrate several influences of pore pressure fields on tensile fracture initiation and propagation. Local pore pressure magnitude contributes directly to the energy available for tensile fracture. A theoretical analysis based on Griffith's strain energy release criteria suggests that tensile fracture is controlled by the general effective stress, $\hat{\sigma}_{ij} = \sigma_{ij} + \alpha p \delta_{ij}$. Experimental data for highly porous limestone and sandstone samples subjected to uniform pore pressure is consistent with this conclusion, but is not precise enough to rule out the conventional effective stress law for tensile failure, $\hat{\sigma}_{ij} = \sigma_{ij} + p\delta_{ij} \geqslant T$.

In non-uniform pore pressure fields, and in the absence of dominating far field stress differences, the strain energy release rate is maximum for tensile fracture propagation towards regions of higher local pore pressure. This has been demonstrated in rock slab experiments in which fractures are propagated either mechanically or hydraulically. Fracture initiation pressure and orientation is influenced not only by differences in local pressure magnitude around the crack tip, but also by the direction of pore pressure gradients. This has been demonstrated with experiments in which a fracture is generated connecting two pressure source ports along a line which is perpendicular to the direction of pressure gradient induced body forces.

In addition to providing insight into basic rock fracture behaviour, the analysis and experiments presented in this paper may contribute to field applications. When *in situ* stresses within a formation do not dominate fracture orientation, or if wells are initially aligned roughly parallel to the maximum compressive stress direction, then hydraulic fractures may be linked by injecting into two or more wells to establish an appropriate pore pressure gradient field before starting fracture operations. A pressurized fracture has also been shown to lower the breakdown pressure of nearby injection ports, a process which can contribute to such linkage. A clear understanding and recognition of pore pressure influence on tensile fracture propagation, both on a local and global scale, is essential when designing efficient fractured line drive or production operations in the field.

Accepted for publication 6 December 1990.

REFERENCES

1. Paterson M. S. *Experimental Rock Deformation—The Brittle Field*, p. 71. Springer-Verlag, Berlin (1978).
2. Hubbert M. K. and Willis D. G. Mechanics of hydraulic fracturing. *Trans. AIME* **210**, 153–163 (1957).
3. Ikeda R. and Tsukahara H. Hydraulic fracturing technique: pore pressure effect and stress heterogeneity. *Int. J. Rock Mech. Min. Sci & Geomech. Abstr.* **26**, 471–475 (1989).
4. Haimson B. C. and Fairhurst C. Hydraulic fracturing in porous-permeable materials. *J. Petrol. Technol.* **21**, 811–817 (1969).
5. Medlin W. L. and Masse L. Laboratory investigation of fracture initiation pressure and orientation. *Soc. Petrol. Engrs J.* **19**, 129–144 (1979).
6. Salz L. B. Relationship between fracture propagation pressure and pore pressure. SPE Paper 6870 presented at the *52nd Annl Fall Meeting of the SPE*, Denver (1977).
7. Felsenthal M. and Ferrell H. H. Fracturing gradients in waterfloods of low-permeability, partially depleted zones. *J. Petrol. Technol.* **23**, 727–730 (1971).
8. Geertsma J. Some rock-mechanical aspects of oil and gas well completions. *Soc. Petrol. Engrs J.* **25**, 848–856 (1985).
9. Detournay E., McLennan J. D. and Roegiers J. C. Poroelastic concepts explain some of the hydraulic fracturing mechanisms. SPE Paper 15262 presented at the *Unconventional Gas Technol. Symp. of the SPE*, Louisville, KY (1986).
10. Rice J. R. and Cleary M. P. Some basic stress diffusion solutions for fluid-saturated elastic porous media with compressible constituents. *Rev. Geophys. Space Phys.* **14**, 227–241 (1976).
11. Jaeger J. C. and Cook N. G. *Fundamentals of Rock Mechanics*, 3rd Edn, p. 214. Chapman & Hall, London (1979).
12. Geertsma J. Problems of rock mechanics in petroleum production engineering. *Proc. 1st Congr. Int. Soc. Rock Mech.*, Lisbon (1966).

Cleary M. P. Rate and structure sensitivity in hydraulic fracturing of fluid-saturated porous formations. *Proc. 20th U.S. Rock Mech. Symp.*, Austin, TX (1979).
14. Boone T. J. and Ingraffea A. R. A numerical procedure for simulation of hydraulically-driven fracture propagation in poro-elastic media. *Int. J. Numer. Anal. Meth. Geomech.* **14,** 27–47 (1990).
15. Bridgeman P. W. Breaking tests under hydrostatic pressure and conditions of rupture. *Phil. Mag.* **24,** 63–80 (1912).
16. Terzaghi K. V. *Theoretical Soil Mechanics*. Wiley, New York (1943).
17. Terzaghi K. V. Stress conditions for the failure of saturated concrete and rock. *Proc. Am. Soc. Test. Mater.* **45,** 777–801 (1945).
18. Biot M. A. General theory of three-dimensional consolidation. *J. Appl. Phys.* **12,** 155–164 (1941).
19. Geertsma J. The effect of fluid pressure decline on volumetric changes of porous rocks. *Trans. AIME* **210,** 331–340 (1957).
20. Cleary M. P. Fundamental solutions for a fluid-saturated porous solid. *Int. J. Solids Structures* **13,** 785–806 (1977).
21. Nur A. and Byerlee J. D. An exact effective stress law for elastic deformation of rocks with fluids. *J. Geophys. Res.* **76,** 6414–6419 (1971).
22. Geertsma J. A remark on the analogy between thermoelasticity and the elasticity of saturated porous media. *J. Mech. Phys. Solids* **6,** 13–16 (1957).
23. Jaeger J. C. Extension failure in rocks subjected to fluid pressure. *J. Geophys. Res.* **68,** 1759–1765 (1963).
24. Schmitt D. R. and Zoback M. D. Laboratory tests of the effects of pore pressure on tensile failure and proposed modification for the hydraulic fracturing breakdown equations in low porosity crystalline rock. *Stanford Rockphysics and Borehole Geophysics Project*, Vol. 37 (1989).
25. Griffith A. A. The phenomena of rupture and flow in solids. *Phil. Trans. R. Soc.* **A221,** 163–198 (1920).
26. Irwin G. R. Fracture dynamics. *Fracturing of Metals*, pp. 147–166. American Society of Metals, Cleveland, OH (1948).
27. Orowan E. Fundamentals of brittle behavior of metals. *Fatigue and Fracture of Metals* (W. M. Murray, Ed.), pp. 139–167. Wiley, New York (1952).
28. Irwin G. R. Analysis of stresses and strains near the end of a crack traversing a plate. *J. Appl. Mech.* **24,** 361–364 (1957).
29. Rice J. R. Mathematical analysis in the mechanics of fracture. *Fracture—An Advanced Treatise*, Vol. II (H. Liebowitz, Ed.), pp. 191–308. Academic, New York (1968).
30. Abou-Sayed A. S., Brechtel C. E. and Clifton R. J. *In situ* stress determination by hydrofracturing: a fracture mechanics approach. *J. Geophys. Res.* **83,** 2851–2862 (1978).
31. Ruina A. Influence of coupled deformation–diffusion effects on the retardation of hydraulic fracture. *Proc. 19th U.S. Rock Mech. Symp.*, pp. 274–282 (1978).
32. Detournay E., Cheng A. H.-D., Roegiers J. C. and McLennan J. D. Poroelasticity considerations in *in situ* stress determination by hydraulic fracturing. *Int. J. Rock Mech. Min. Sci. & Geomech. Abstr.* **26,** 507–513 (1989).
33. Kannenen M. F. and Popelar C. H. *Advanced Fracture Mechanics*, pp. 159–162. Oxford University Press, New York (1985).
34. Haimson B. and Fairhurst C. *In situ* stress determination at great depth by means of hydraulic fracturing. *Proc. 11th U.S. Symp. on Rock Mech.*, Berkeley, CA, pp. 559–584 (1970).
35. Lo K. K. Analysis of branched cracks. *J. Appl. Mech.* **45,** 797–802 (1978).
36. Goodier J. N. Compression of rectangular blocks, and the bending of beams by non-linear distribution of bending forces. *Trans. Am. Soc. Mech. Engrs* **53,** 173–183 (1932).